MDPI

Article

A New Lead-Free Copper Alloy CuAl8Fe5Ni4Zn4Sn1 for Plain Bearings and Its Strengthening Mechanisms

Björn Reetz * and Tileman Münch

OTTO FUCHS Dülken GmbH & Co. KG, 41751 Viersen, Germany; tileman.muench@otto-fuchs.com
* Correspondence: bjoern.reetz@otto-fuchs.com

Abstract: CuAl8Fe5Ni4Zn4Sn1 (OF 2238) is a new lead-free copper alloy for plain-bearing applications that was first officially presented in a scientific journal in 2020. Soon after its invention, the use of the alloy for connecting rod bushings in heavy-duty internal combustion engines was promoted and validated with customers. The aim of this article is to describe the material properties of the new alloy in more detail than previously and explain how the advantageous properties of CuAl8Fe5Ni4Zn4Sn1 are generated. At the beginning of this article, the general development trends in the field of copper alloys for sliding applications are presented, into which the new alloy from this publication can be classified. In the main part of this publication, the authors go through the production chain of CuAl8Fe5Ni4Zn4Sn and show how the entire manufacturing process contributes to obtaining a material with a combination of high strength, ductility and sufficient toughness. This starts with fine microstructures after casting, followed by homogenisation and refinement during hot extrusion and work hardening chiefly during cold drawing. What is most surprising, however, is the finding that a strong hardening effect can be achieved in the new alloy by precipitation of fine κ-phase at temperatures of about 400 °C and air cooling without prior solution treatment. These results make it clear that there is great potential for further material developments to support material efficiency and even to expand the application limits.

Keywords: multi-constituent bronze copper alloys; heavily loaded sliding applications; strengthening mechanisms

1. Current Copper Materials and Development Trends of New Copper Alloys for Sliding Applications

The family of traditional copper wrought alloys for sliding applications includes a wide range of chemical compositions, including CuNiSi alloys, nickel–aluminium bronze and tin bronze, binary CuZn alloys with and without lead, silicon–brass alloy CuZn31Si1 and special brass alloys [1–3]. Many of them have been used for decades without significant changes in their chemical compositions and microstructures.
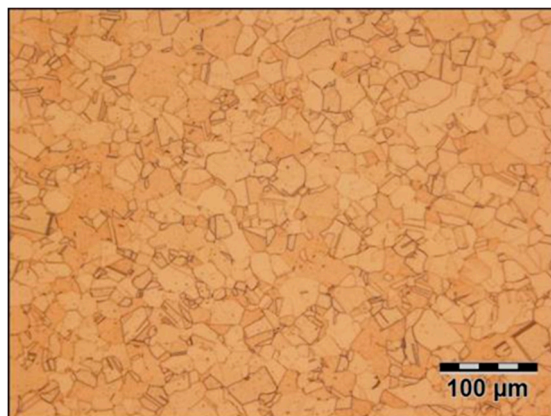
For several reasons, these alloys traditionally are alloyed with far more than 0.1% lead by mass. The lead content ranges from 0.1 to 2 mass-% in special brass alloys (e.g., CuZn37Mn3Al2Pb Si), up to 3.5 mass-% in brass alloys for machining [4] and even up to 23 mass-% in lead bronze alloys for sliding applications [5]. As an alternative for these applications, a wear-resistant layer of tin bronze with PTFE as a solid lubricant can be applied on a different base material, e.g., on aluminium or steel [6,7].

For vehicles, the End-of-Life Vehicles Directive 2000/53/EU restricts the use of hazardous substances such as lead. Although the End-of-Life Vehicles Directive 2000/53/EU still defines exemptions for restricted substances such as lead, no one can be sure that the exemptions will ever end. In this context, the European Commission (EC) also began setting limits for dangerous substances such as cadmium, mercury and lead around 2000 [8]. In 2018, the European Commission approved the decision to classify lead as toxic to reproduction [9]. After that, the development of new lead-free alloys for sliding applications accelerated substantially.
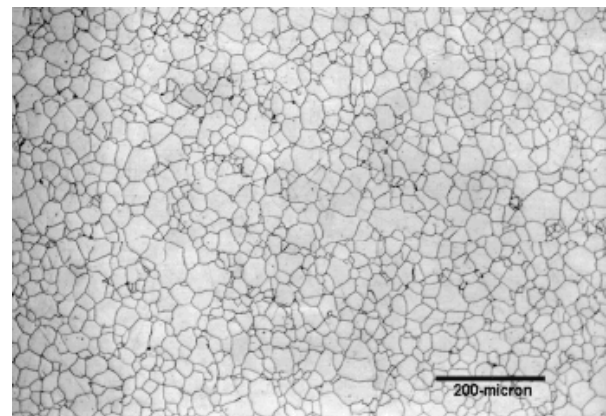
The latest development in hazardous substances regulation is a proposal to ban the use of PFAS. The result of this would be that an important solid lubricant would also be banned from sliding materials.

Based on the developments described above, it is not surprising that copper alloy manufacturers and consumers are becoming increasingly active in developing and validating alternative lead-free copper alloys (e.g., see [10]).
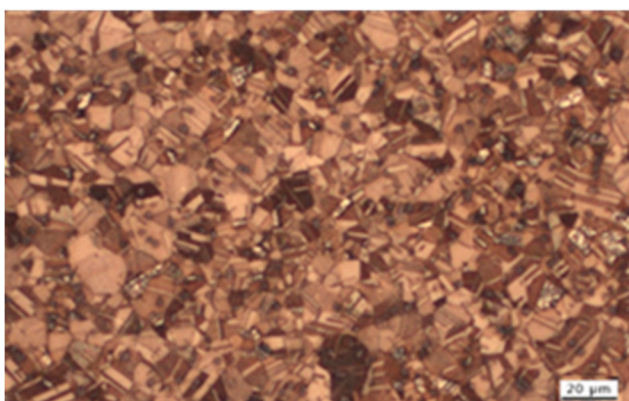
However, the new developments in lead-free copper alloys can only be properly understood by looking at the wrought copper alloys already available for sliding applications from the past. The family of existing standardised wrought alloys for sliding applications includes several bronze and brass special brass alloys. Typical bronze alloys for this are CuNi2Si [11], CuNiSn-alloys (e.g., CuNi6Sn6 and CuNi15Sn8 [12]), CuSn8 [13]/CuSn8P and CuAl10Ni5Fe4 [14] (Figure 1). All of these bronze alloys have a high proportion of alpha phase and alloying elements such as aluminium, nickel or tin. This leads to good mechanical wear resistance, quite high-temperature stability and good corrosion resistance. Mechanical strength and fatigue strength depend heavily on the work-hardening state of these alloys and can therefore be increased significantly by cold forming [15]. Further properties relate to individual bronze alloys. In the case of CuNi2Si, the specific properties are a combination of excellent mechanical properties with good electrical and thermal conductivity [16]. Another example is tin in CuSn8/CuSn8P. The formation of tin oxide layers in frictional contact promotes the good friction and wear properties of this alloy [17].
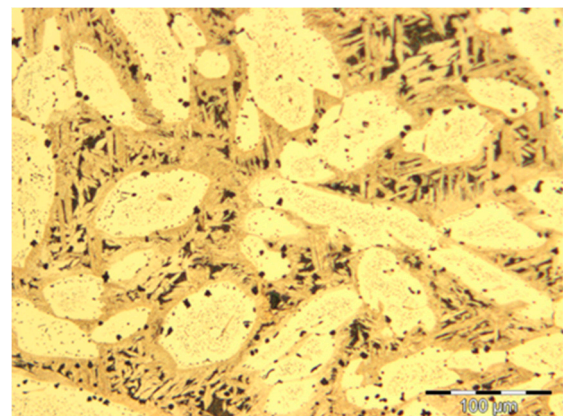

(**a**)

(**b**)

(**c**)

(**d**)

Figure 1. Typical micrographs of different bronze alloys for sliding applications: (**a**) CuNi2Si, reprinted with permission from reference [11] Copyright OTTO FUCHS Dülken; (**b**) CuNi15Sn8, reprinted with permission from reference [12] Copyright STAINLESS; (**c**) CuSn8P reprinted with permission from reference [13] Copyright Schmitz-Metallographie; and (**d**) CuAl10Ni5Fe4, reprinted with permission from reference [14] Copyright OTTO FUCHS Dülken.

Typical standardised brass alloys for sliding applications with very low loadings are CuZn40/CuZn42 and, respectively, CuZn39Pb3/CuZn40Pb2 (Figure 2a) [15]. The microstructures of CuZn40 and CuZn39Pb3 consist of a pure β/α matrix and are free of any hard phases that could protect against wear. This is the reason why such alloys are only used for very moderate loads. CuZn39Pb3 and CuZn40Pb2 are obviously lead-alloyed, but traditionally, CuZn40/CuZn42 also contain more than 0.1 mass-% lead for improvement of machinability.

(a)

(b)

(c)

Figure 2. Typical micrographs of different brass alloys for sliding applications: (**a**) CuZn40Pb2; (**b**) CuZn31Si1; and (**c**) CuZn37Mn3Al2PbSi, reprinted with permission from reference [18] Copyright OTTO FUCHS Dülken.

CuZn31Si1 alloys (both lead-alloyed and lead-free, silicon brass) are used as a standard for low- to medium-load-sliding applications (Figure 2b) [15]. These silicon brasses have a structure consisting predominantly of the α-brass phase with a smaller proportion of the β-brass phase, which is aligned in the direction of hot deformation. Compared with the α-phase, the β-phase contributes more to the wear resistance of this alloy. The silicon in this alloy is kept in a solid solution.

When brass alloys with increased wear resistance are required, normally, special brass alloys such as CuZn37Mn3Al2PbSi (Figure 2c) are chosen [15,18]. Using the variation in the chemical composition, the resulting zinc equivalent and the temperature treatment of the materials, the brass matrix in such alloys can be adjusted from predominantly α-phase to a mixture of α- and β-phases to pure β-phase. In brass alloys, a higher content of the β-phase already leads to better wear resistance, but the main effect is achieved by the hard phase particles (usually silicides with a length of a few μm to a maximum of several 100 μm) which are distributed homogeneously within the brass matrix to protect the softer brass matrix from wear.
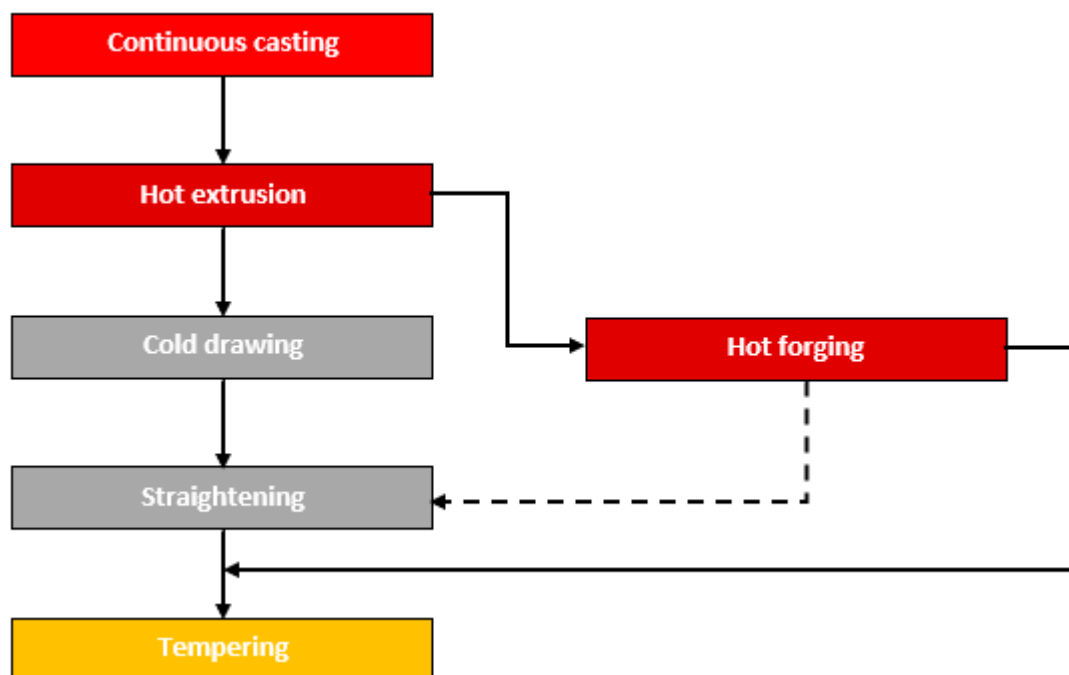
For every development of new copper-based sliding alloys, the existing materials are the benchmark that must at least be met if not exceeded. However, there are two

fundamentally different ways to develop new lead-free copper alloys for sliding applications [19–22]. On the one hand, the inventor can start from an existing alloy and improve it through iterative steps of chemical and processing measures. An example is the alloy CuZn31Si1, which originally contained 0.3 to 0.8% lead by mass. With the only goal to be lead-free, the lead content could be limited to a maximum of 0.1% by mass. However, the absence of lead not only deteriorates the machinability of CuZn31Si1 but does not contribute to improving the modest load capacity of the alloy either. Consequently, further improvements in CuZn31Si1 aim to increase its wear resistance by alloying certain amounts of manganese and silicon. Likewise, the wear resistance of special brass alloys of type CW713R can be improved by varying the Al, Mn, Ni and Si content (e.g., see [23]).

On the other hand, the invention of new alloys can be based on completely new concepts. As an example, it has been possible to use new Cu-Al-Mn-Zn alloys to replace nickel silver in sliding applications [24]. The newest trend is high-entropy alloys, which go completely beyond the existing copper alloy families. This concept is also being considered for innovative alloys in sliding applications [25].

Finally, the alloy composition and α/β-phase mixture also have a strong effect on the production process for manufacturing semi-finished parts for sliding applications (Figure 3) [26]. In the hot extrusion and hot forging processes, a high β content helps reduce hot forming resistance. For cold forming steps such as cold drawing and straightening of bars, tubes or forgings, cold stamping or flanging a higher α-phase content facilitates the forming process.

Figure 3. Production steps in manufacturing pre-material tubes for radial bearings.

To combine all these benefits, the concept for the new alloy was to have sufficient β-phase for good hot formability during extrusion at about 900 °C, while the β-phase should be transformed to α-phase when the alloy is cooled down to room temperatures after that. The α-phase is needed to support the cold drawing and straightening that follow after hot extrusion.

2. Materials and Methods of Investigation

This new alloy is a new multi-component bronze alloy from OTTO FUCHS Dülken, Germany with the short name CuAl8Fe5Ni4Zn4Sn1. The chemical composition (Table 1) differs from any conventional family of standardised bronze alloys. The basic idea for
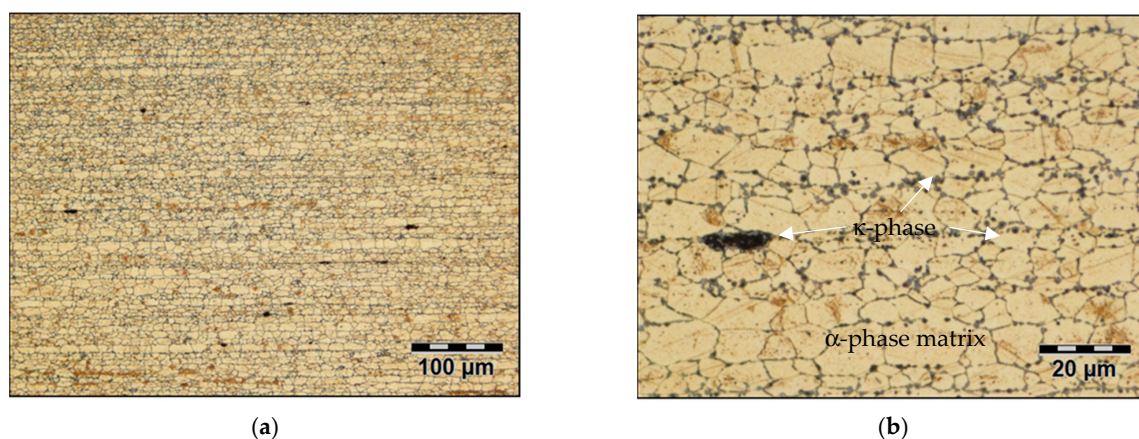
designing the new alloy was to combine the positive effects of the alloying strategy of other bronze alloys such as aluminium bronze, tin bronze and CuZn gliding metal. The copper content of CuAl8Fe5Ni4Zn4Sn1 is at least 75 mass-%, and the sum of all alloying elements is in the range of 17 to 25 mass-%. With the chosen combination of aluminium, zinc and tin as alloying elements, stable tribolyers for improving load capacity are achieved [27,28]. An additional advantage of this alloy is that it is technically lead-free (maximum 0.1 mass-% lead).

Table 1. Chemical composition of alloy CuAl8Fe5Ni4Zn4Sn1 with the specified limits. Values are given in mass-%.

	Cu	Zn	Pb	Sn	Fe	Mn	Ni	Al
Min	balance	3.0	-	0.5	3.5	-	3.0	7.0
Max	-	5.0	0.1	2.0	5.5	0.5	5.0	9.0

The microstructures of CuAl8Fe5Ni4Zn4Sn1 after complete manufacturing including continuous casting, hot extrusion, cold drawing and tempering consist of a homogeneous α-brass matrix in which numerous fine and individual coarser intermetallic κ-phases are embedded (Figure 4).

(**a**)   (**b**)

Figure 4. Micrographs of CuAl8Fe5Ni4Zn4Sn1 with two different magnifications. Longitudinal section. Material condition is hot extruded, cold drawn and finally tempered. Overview (**a**) and detail picture (**b**).

According to the various physical, mechanical and technological requirements for the new alloy CuAl 8Fe5Ni4Zn4Sn1, the following characteristic mechanical properties were identified for the pre-material for plain radial bearings. These characteristics are given in Table 2 and can also be found in the first publication [29] and in the material data sheet [30].

Table 2. Characteristic requirements on the mechanical properties of CuAl8Fe5Ni4Zn4Sn1 for bushings for bearings (at room temperature).

Mechanical Property	Unit	Requirement *
0.2%-Yield strength	MPa	Minimum 500
Tensile strength	MPa	Minimum 700
Elongation at fracture	%	Minimum 5
Hardness Brinell	HBW	210
Bending fatigue strength	MPa	~220 to 230

* For information only.

In this publication, the progress in the further development of the alloy is presented. Compared with the first publication in 2020 [29], a much deeper understanding of the
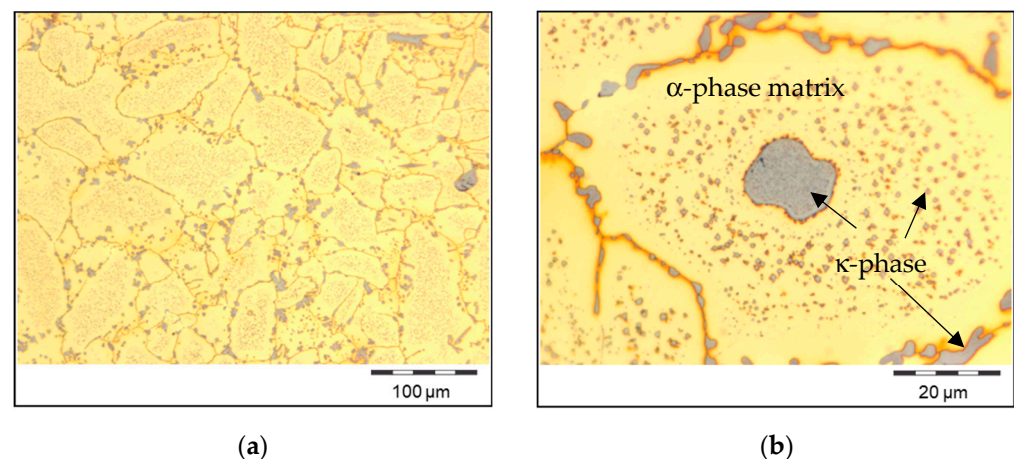
strengthening mechanisms of the new alloy was achieved, which is the subject of this publication. For this purpose, tubes and rods made of CuAl8Fe5Ni4Zn4Sn1 were produced on the same series of machines and in the same way as for plain bearing customers. Using the bar material, the influence of the degree of cold deformation during drawing on the room temperature hardness and the resulting tensile properties was examined. The tube material was used again to examine the tempering parameters. Thus, the final tempering was not only carried out in an industrial furnace but also with pipe sections at different tempering temperatures in a laboratory furnace. Temperatures between 380 and 650 °C were used in the tempering trials.

For microstructure characterization, light optical microscopy (LOM) was carried out after each manufacturing step. Sample preparation of the sections included cutting, mounting, rough grinding and fine grinding, polishing and etching with iron-III-chloride. Micrographs were then taken using an Olympus Bx51M microscope equipped with an Olympus DP73 camera at OTTO FUCHS Dülken, Germany. Electron microscopy was also performed before and after tempering using FEI Apreo with AZtecLive for elemental analysis which is available in the laboratory of OTTO FUCHS Meinerzhagen, Germany. For the tensile test at room temperature according to DIN EN ISO 6892-1 [31], a Zwick Roell testing device Z100 (in the case of round samples made of rod material) or a spindle testing machine from Wolpert (in the case of flat samples made of tube material) from OTTO FUCHS Dülken, Germany was used. A Zwick Roell DuraVision device from OTTO FUCHS Dülken, Germany was available to determine Brinell hardness.

3. Results and Discussion of the Strengthening Mechanisms of CuAl8Fe5Ni4Zn4Sn1

3.1. Initial Condition after Continuous Casting

Continuous casting is the first production step in the manufacturing route of OF 2238 pre-material tubes (bigger diameter) and rods (smaller diameter) for bushings. Choosing the right casting parameters, e.g., in terms of casting temperature and casting speed, these bars already provide very fine-grained and homogeneous microstructures of the α-matrix phase. These grains are elongated only near the outer surface. The rest of the cross-section consists of fine globular matrix grains. In the interior and on the grain boundaries of the α-grains, κ-phase precipitations are present. The distribution of the κ-phase is nearly homogeneous (Figure 5).

(a)   (b)

Figure 5. Micrographs of CuAl8Fe5Ni4Zn4Sn1 with magnification 100× (**a**) and 1000× (**b**). Cross-section. The material condition is a continuous cast bar.
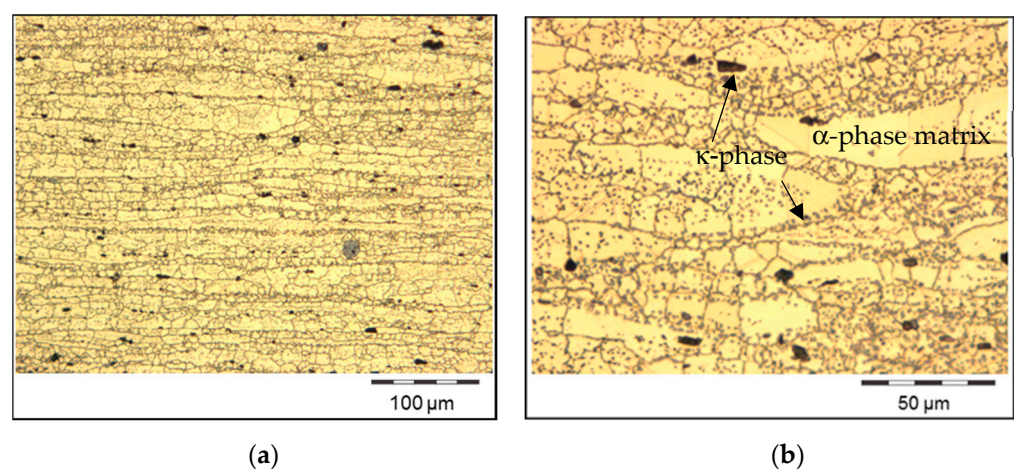
These microstructures are different compared with the dendritic morphology typically found in other bronze alloys such as tin bronze [32] or the standard nickel–aluminium bronze [33,34]. This is caused by several reasons including the following:

- CuAl8Fe5Ni4Zn4Sn1 is a polymorph alloy with a β-phase during solidification, which transforms into the α- and κ-phases during cooling to room temperature [35]. In such an alloy, the solid–solid phase transformation during cooling after solidification has an additional impact on grain refinement. This is because a plurality of daughter grains can result from each mother grain. The same behaviour can be observed in other polymorph copper alloys such as α/β brass [26].
- The iron content further contributes to the refinement of the microstructures. This effect is related to the iron, which is in solid solution in the copper matrix, as this proportion supports nucleation [36].
- The aforementioned aspects count for other bronze alloys such as CuAl10Ni5Fe4 as well. Notwithstanding that, as-cast CuAl10Ni5Fe4 also provides fine grains but a dendritic grain morphology. In comparison, CuAl8Fe5Ni4Zn4Sn1 does not only provide fine but also globular microstructures. Therefore, further differences in the chemical compositions must be the reason for the globular microstructures of CuAl8Fe5Ni4Zn4Sn1.
- Most likely, the globular microstructures of CuAl8Fe5Ni4Zn4Sn1 can be explained by the effect of tin, which is reported to shift the grain morphology of aluminium bronze to globulitic. This is due to the decline in nucleation temperatures, the reduction in undercooling intensity and the decrease in cooling rate during solidification [37].

To conclude this paragraph, the fine and globular microstructures of the alloys are the result of solidification behaviour, phase transformations and nucleation effects. Starting with fine-casting microstructures is also beneficial for promoting fine microstructures in the finished wrought alloy product and, therefore, starting with these microstructures in the first production step provides strength to the raw material bars.

3.2. Hot Extrusion of Rods and Tubes

Dynamic recrystallisation during hot extrusion leads to homogenisation and additional refinement of the microstructures from casting [38]. After hot extrusion, the microstructures consist of an α-phase matrix with κ-phase precipitations, the latter having a size of several microns. The grains are stretched in the extrusion direction, while the grain size in the radial direction is smaller (Figure 6). However, the grain size is also significantly smaller in the transverse direction compared with the cast state. The decrease in grain size compared with the as-cast state is the main reason for the increased strength after hot extrusion (Hall–Petch relationship [39–41]). The Hall Petch effect is more pronounced in longitudinal than in transverse direction because of the aspect ratio of the grains.
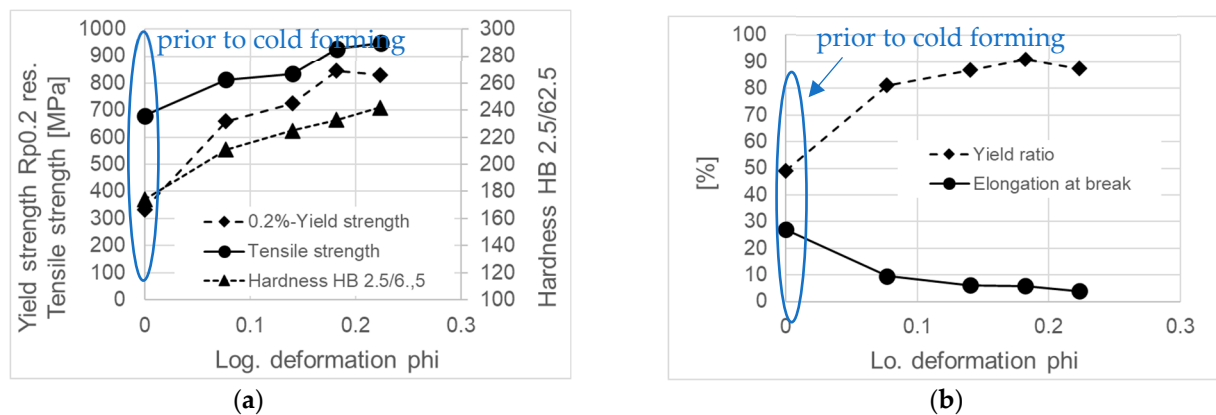

(**a**)　　　　　　　　　　　　　(**b**)

Figure 6. Micrographs of CuAl8Fe5Ni4Zn4Sn1 with two magnification 100× (**a**) and 200× (**b**). Longitudinal section. The material condition is an extruded tube.

Another strengthening mechanism comes from work hardening during hot extrusion. So, there are two mechanisms that result in a higher strength of the extruded product compared with the cast billet.

3.3. Effect of Cold Drawing and Straightening of the Extruded Tubes

After hot extrusion, the tubes are cold drawn and straightened for dimensional reasons (increasing straightness and reducing diameter tolerance) and to increase mechanical strength. The cold strengthening effect is shown in Figure 7.

Figure 7. Mechanical properties of CuAl8Fe5Ni4Zn4Sn1 after continuous casting, followed by hot tube extrusion and cold drawing depending on the deformation degree of cold drawing, yield strength, tensile strength and hardness (**a**) as well as the yield ratio and elongation at break (**b**).

Similar to nickel alloys and austenitic steels, in this new bronze alloy, the deformation of the fcc lattice of the α-phase generates substantial work hardening. The work-hardening effect is enhanced by aluminium, tin and zinc, which are in solid solution [15]. By this, CuAl8Fe5Ni4Zn4Sn1 achieves in the cold-drawn condition strength values similar to or even higher than those typically known for other bronze alloys such as CuAl10Ni5Fe4.
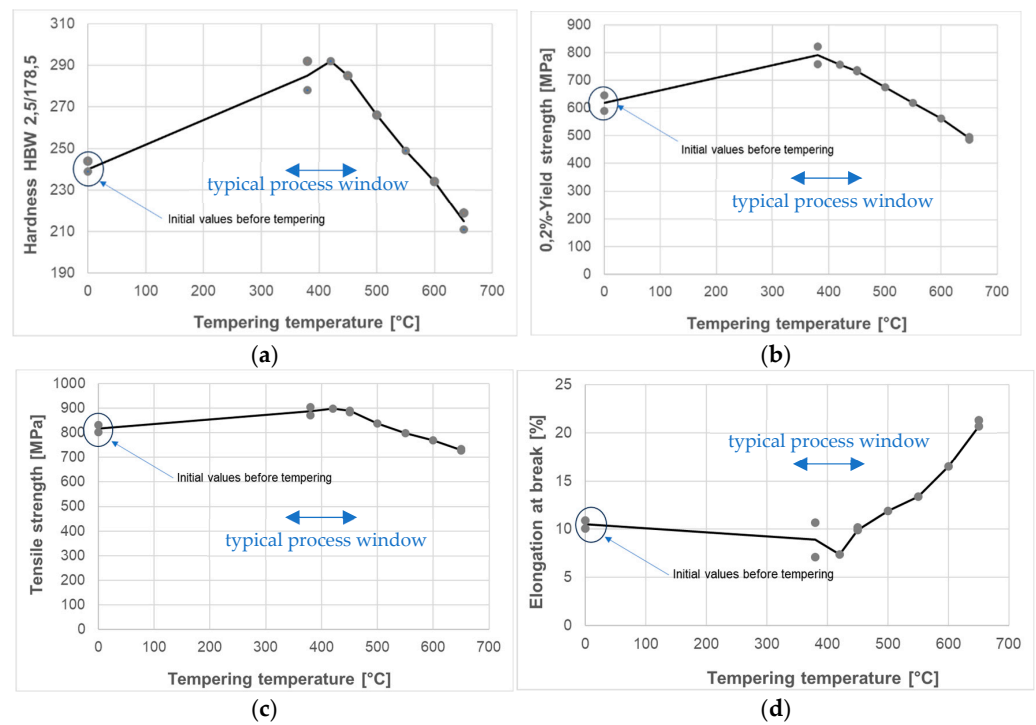
3.4. Thermal Treatment after the Cold Drawing of CuAl8Fe5Ni4Zn4Sn1

The deformation in the cross-section during cold drawing is inhomogeneous. The main reasons are the friction between the tool surface and the tube material, heating and local differences in the stress state [42] are the following:
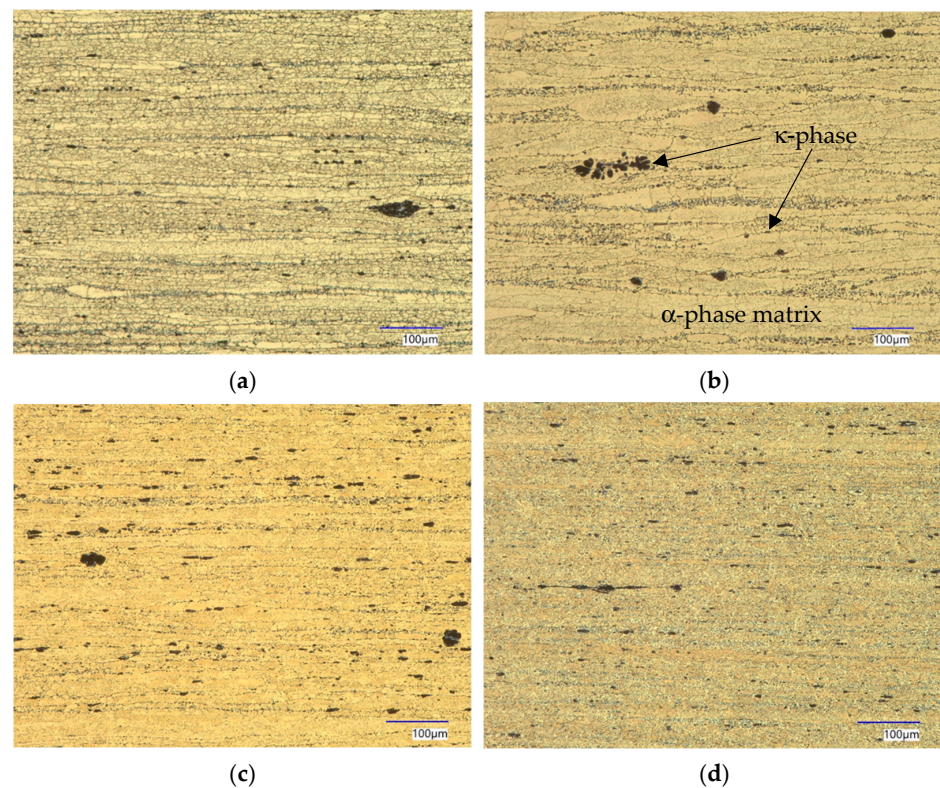
- Shear deformation in the near-surface zones of the tube material occurs because of the friction between the tool surface and the tube material;
- Furthermore, being surrounded by the neighbouring material in all directions results in a triaxial stress state of the core, but the stress state near the tube surface is nearly plane;
- Both the aforementioned friction and adiabatic heating lead to increasing temperatures in the tube material. Therefore, the temperature distribution in the tube cross-section is also inhomogeneous.

After cold drawing, most of these stresses remain in the material [43,44]. But depending on the type (tensile or compressive) and magnitude, residual stresses can subsequently have a negative impact on the processing and use of the tubes (distortion, stress cracking, relaxation and Bauschinger effect, to name just a few examples). Thus, they must be reduced, which is achieved for CuAl8Fe5Ni4Zn4Sn1 by tempering with air cooling.

Typically, the tempering temperature for aluminium bronze alloys is between 350 and 650 degrees Celsius. This range was also covered in the tempering tests of CuAl8Fe5Ni4Zn4Sn1 (Figure 8). Considering the light optical micrographs, no significant effect on the microstructures after different tempering temperatures is found (Figure 9).
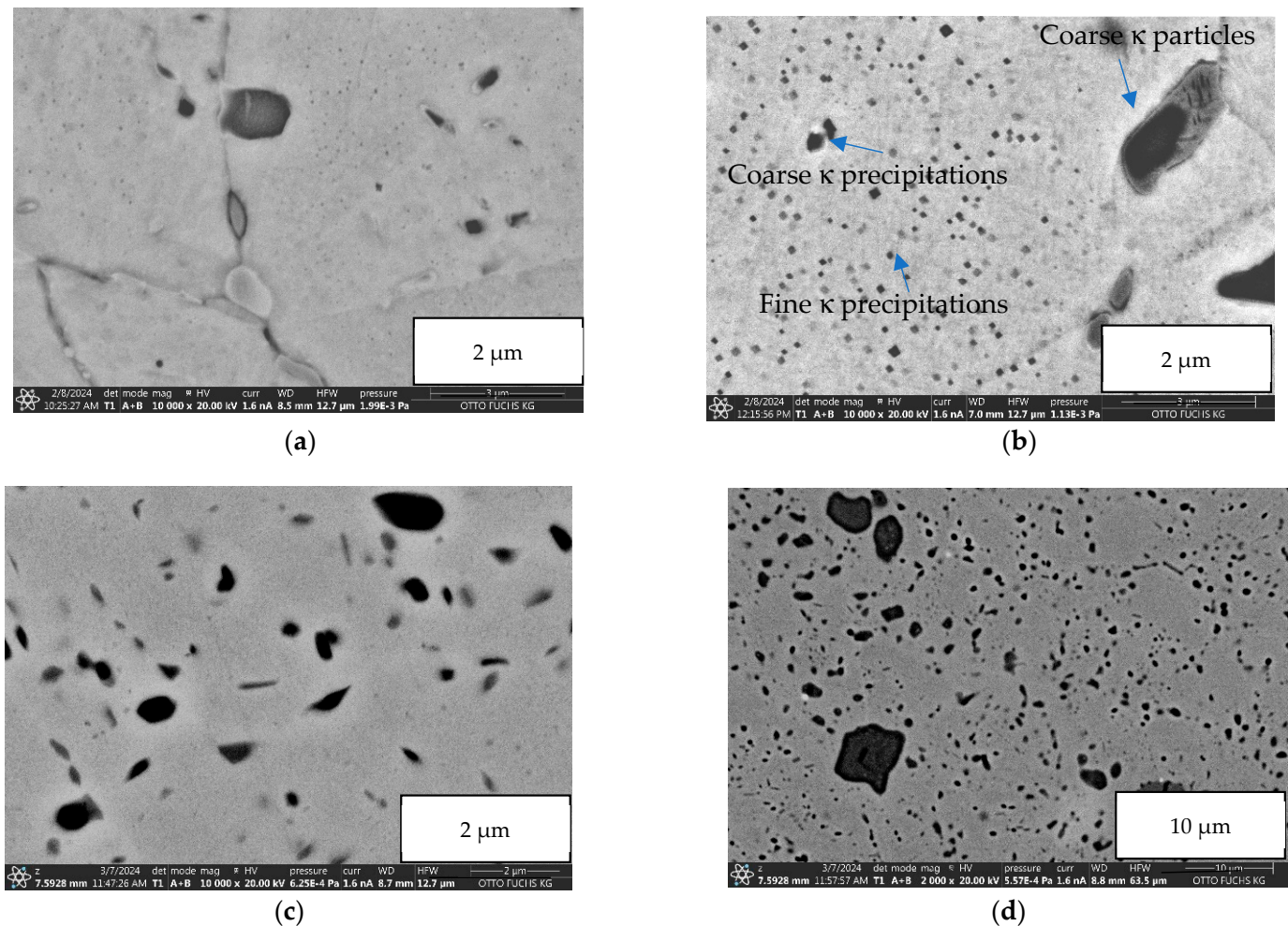
Figure 8. Mechanical properties of CuAl8Fe5Ni4Zn4Sn1 depending on tempering temperature (3 h tempering time): (**a**) hardness, (**b**) 0.2%-yield strength, (**c**) tensile strength and (**d**) elongation at break. The material was previously hot extruded, cold drawn and straightened.

Figure 9. Micrographs from light optical microscopy of CuAl8Fe5Ni4Zn4Sn1 before (**a**) and after tempering with (**b**) 420 °C, (**c**) 500 °C and (**d**) 650 °C, 3 h tempering time. The material was previously hot extruded, cold drawn and straightened.
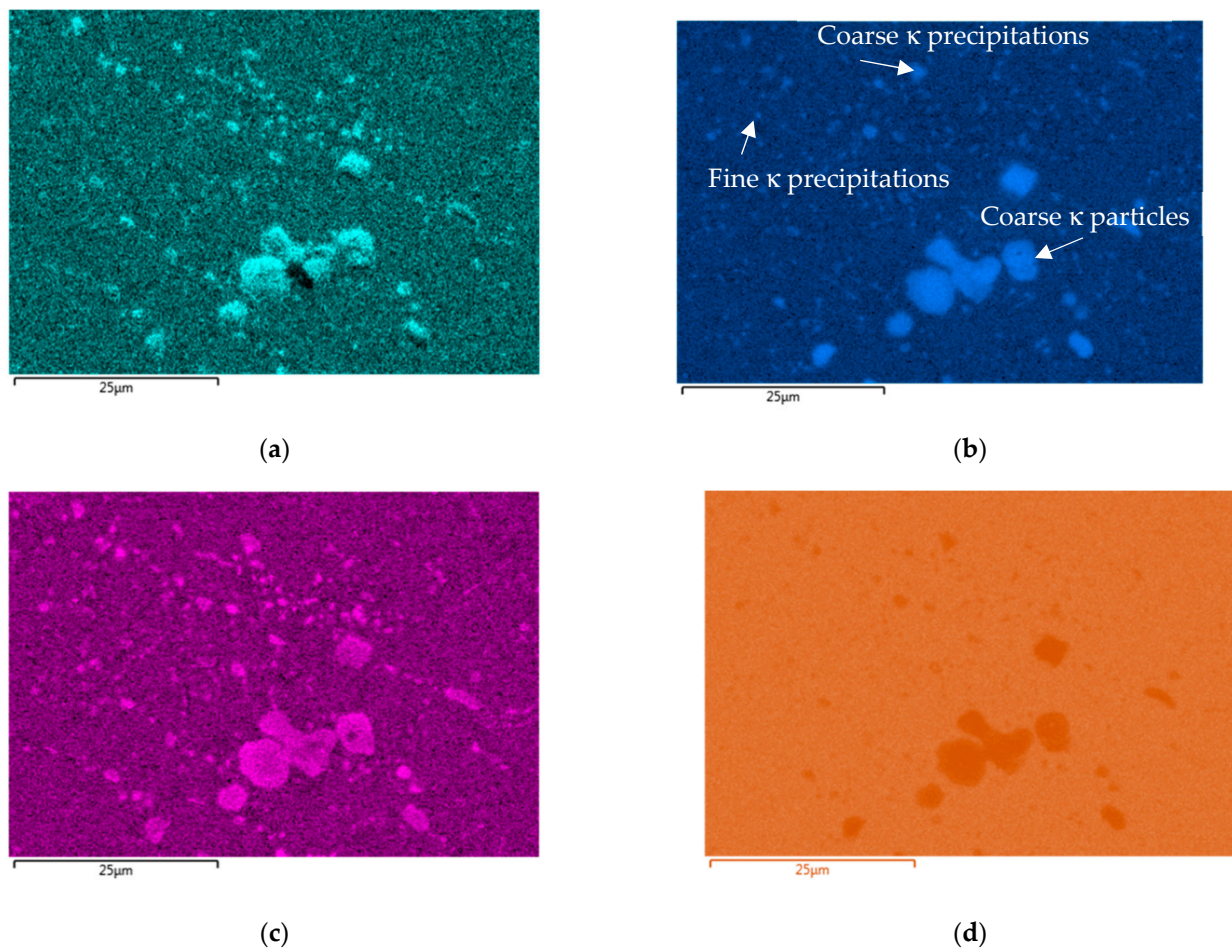
However, the tempering tests had an unexpected result. It can be seen from the diagram that the new alloy shows age hardening. In other aluminium–bronze alloys, age hardening is only achieved if the material has undergone a solutionising process previously. For CuAl8Fe5Ni4Zn4Sn1, the age hardening of the alloy can be carried out without this heating process and yet, the increase in strength is at least similar or even higher than with solution-annealed CuAl10Ni5Fe4. In order to find the reason for this effect the material was analysed by surface electron microscopy (Figure 10).

Figure 10. SEM images of CuAl8Fe5Ni4Zn4Sn1 before (**a**) and after tempering with (**b**) 420 °C, (**c**) 500 °C and (**d**) 650 °C, 3 h tempering time. The material was previously hot extruded, cold drawn and straightened.

Both coarse and fine precipitations (κ-phases) can be seen and were analysed using EDX mapping (Figure 11) and point analysis. As shown in Table 3, coarse particles are of the Fe$_3$Al-type, but because of their size of several microns, they have only little relevance for the strengthening of the material. The size of the fine particles ranges from about 20 to 100 nm, and they are of the Fe$_3$Al-, NiAl- and Al$_3$Ni$_5$-types. This means that these fine precipitates are just the right size for effective precipitate hardening, and these results demonstrate that fine κ-phase precipitations are the reason for such strong age hardening in the new alloy.

Figure 11. Qualitative illustration of the element distribution of (**a**) aluminium, (**b**) iron, (**c**) nickel and (**d**) copper, derived from EDX-mapping of CuAl8Fe5Ni4Zn4Sn1 after tempering with 550 °C. The brighter the colour, the higher the content of the element. The material was previously hot extruded, cold drawn and straightened.

Table 3. Chemical composition according to EDX measurements at different locations of the microstructures of CuAl8Fe5Ni4Zn4Sn1.Values are given in atom-% (also see Figure 8).

	Cu	Zn	Sn	Fe	Ni	Al
Matrix	74	4	1	3	3	15
Coarse particles (centre)	16	0	0	50	14	20
Coarse particles (outer edge)	32	0	0	14	22	32
Coarse precipitations (Fe-rich)	13	0	0	47	14	26
Coarse precipitations (Ni-rich)	50	3	0	19	22	6
Fine precipitations (Fe-rich)	67	0	0	23	10	0
Fine precipitations (Ni-rich)	83	5	0	3	5	4

4. Conclusions and Outlook

CuAl8Fe5Ni4Zn4Sn1 is a new copper-based alloy for plain-bearing bushings where high strength is required. The bushing manufacturing route begins with the continuous casting of bars for billets. The following process steps are hot extrusion, cold drawing, straightening and tempering. The authors have shown how the entire manufacturing process contributes to obtaining a material with a combination of high strength, ductility and sufficient toughness. Starting with fine microstructures after casting, homogenisation and refinement occur during hot extrusion. Some work hardening effects are related to hot forming and particularly cold drawing.

The most unexpected impact on material strength was achieved by tempering the cold-formed tubes. Without previous solutionising, there is a strong hardening effect in the new alloy by precipitation formation of the κ-phase at temperatures of about 400 °C and air cooling.

It can be stated that the new chemistry of CuAl8Fe5Ni4Zn4Sn1 with the chosen amounts of Sn, Fe and Ni together with a carefully designed production process leads to a big advantage in comparison with other aluminium bronze alloys like CuAl10Ni5Fe4 or others. Neither solutionising prior to age hardening nor quenching is necessary to obtain these excellent results.

The existing copper alloys, which were developed previously, have been used for many years. The situation changed when the banishment of lead from these alloys spurred the development of new copper alloys. As can be seen from the development of CuAl8Fe5Ni4Zn4Sn1 [26], the new copper alloys are a serious alternative to the existing standard alloys. This new development makes clear that many unexplored alloy combinations could display further unexpected benefits.

References

1. Arens, J.; Bungardt, W.; Mann, H.; Martin, E.; Meboldt, W.; Meysenbug, C.M.; Thum, A.; Weber, R.; Wiemer, H.; Kühnel, R. *Werkstoffe für Gleitlager*; Springer-Verlag OHG: Berlin/Göttingen/Heidelberg, Germany, 1952; pp. 233–318.
2. Welsh, R.J. *Plain Bearing Design Handbook*; Butterworths University of California: Los Angeles, CA, USA, 1983.
3. Koring, R. *Changes in Plain Bearing Technology*; SAE International: Warrendale, PA, USA, 2012.
4. Deutsches Kupferinstitut. Kupfer-Zink-Legierungen (Messing und Sondermessing). Available online: https://kupfer.de/wp-content/uploads/2019/09/i5.pdf (accessed on 8 March 2024).
5. Dinesh, D.; Megalingam, A. Dry Sliding Friction and Wear Behaviour of Leaded Tin bronze for Bearing and Bushing Application. *Arch. Metall. Mater.* **2021**, *66*, 1095–1104. [CrossRef]
6. Bartz, W.J. *Selbstschmierende und wartungsfreie Gleitlager. Typen, Eigenschaften, Einsatzgrenzen und Anwendungen*; Expert-Verlag: Tübingen, Germany, 1993.
7. Jose, J.P.; Thomas, S.; Kuruvilla, J.; Malhotra, S.K.; Goda, K.; Sreekala, M.S. Advances in polymer composites: Macro- and microcomposites—State of the art, new challenges, and opportunities. In *Polymer Composites*; Wiley: Weinheim, Germany, 2012; Volume 1, pp. 3–16.
8. Directive 2002/95/EC of the European Parliament and of the Council of 27 January 2003 on the Restriction of the Use of Certain Hazardous Substances in Electrical and Electronic Equipment. Available online: https://eur-lex.europa.eu/LexUriServ/LexUriServ.do?uri=CELEX:32002L0095:en:PDF (accessed on 7 June 2024).
9. Available online: https://echa.europa.eu/documents/10162/61ac8d81-6ea2-6ad0-ffef-95037c9182ce (accessed on 11 March 2024).
10. Reetz, B.; Münch, T. Challenges for novel lead-free alloys in hydraulics. In Proceedings of the 12th International Fluid Power Conference, Dresden, Germany, 12–14 October 2020; Available online: https://tud.qucosa.de/api/qucosa:71055/attachment/ATT-0/ (accessed on 11 March 2024).
11. OTTO FUCHS Dülken, 2022, internal metallographic investigation, more information available from OTTO FUCHS Dülken on request only.
12. Stainless, Technical Data Sheet. Available online: https://www.stainless.eu/wp-content/uploads/2023/03/ToughMet3-ALL.pdf (accessed on 13 May 2023).
13. Schmitz Metallographie GmbH. Available online: https://www.schmitz-metallographie.de/gefuge/cw453k-cusn8-2/ (accessed on 23 May 2024).
14. Gummert, H.; Reetz, B. Anwendungsoptimierte Kupfer-Knetlegierungen für Gleit-und Wälzlager. *Metall* **2015**, *11*, 463–467. Available online: https://kupfer.de/wp-content/uploads/2019/11/463-FA-Reetz.pdf (accessed on 13 May 2024).

15. Dies, K. *Kupfer und Kupferlegierungen in der Technik*; Springer: Berlin/Göttingen/Heidelberg, Germany, 1967.
16. Shalunov, E.; Shalunov, S.; Vladimirova, Y. Analysis of Operating Conditions of Heavy-Loaded and Heat-Stressed Friction Units of Powerful Internal Combustion Engines and Development of Copper Nanocomposite Powder Materials for Them. MATEC Web of Conferences 298 (2019). Available online: https://www.matec-conferences.org/articles/matecconf/pdf/2019/47/matecconf_icmtmte18_00101.pdf (accessed on 11 March 2024).
17. Collini, L. Copper Alloys-Early Applications and Current Performance-Enhancing Processes; InTech, Croatia. 2012. Available online: http://www.issp.ac.ru/ebooks/books/open/Copper_Alloys_-_Early_Applications_and_Current_Performance_-_Enhancing_Processes.pdf (accessed on 11 March 2024).
18. OTTO FUCHS Dülken, 2024, internal metallographic investigation, more information available from OTTO FUCHS Dülken on request only.
19. Miracle, D.B. Critical Assessment 14: High entropy alloys and their development as structural materials. *Mater. Sci. Technol.* **2015**, *31*, 1142–1147. [CrossRef]
20. Miracle, D.B.; Senkov, O.N. A critical review of high entropy alloys and related concepts. *Acta Mater.* **2017**, *122*, 448–511. Available online: https://www.sciencedirect.com/science/article/pii/S1359645416306759 (accessed on 13 May 2024). [CrossRef]
21. Wang, C.; Fu, H.; Jiang, L.; Xue, D.; Xie, J. A property-oriented design strategy for high performance copper alloys via machine learning. *Comput. Mater.* **2019**, *5*, 87. Available online: https://www.nature.com/articles/s41524-019-0227-7 (accessed on 13 May 2024). [CrossRef]
22. Anamu, U.S.; Ayodele, O.O.; Olorundaisi, E.; Babalola, B.J.; Odetola, P.I.; Ogunmefun, A.; Ukoba, K.; Jen, T.-C.; Olubambi, P.A. Fundamental design strategies for advancing the development of high entropy alloys for thermo-mechanical application: A critical review. *J. Mater. Res. Technol.* **2023**, *27*, 4833–4860. [CrossRef]
23. OTTO FUCHS Dülken Material Data Sheets: Alloy OF 2228, available from OTTO FUCHS Dülken on request.
24. Jitchoom, S.; Rojananan, S.; Rojananan, S. Influence of Aluminium on the Color, Microstructure and Hardness of White Alloys. *Adv. Mater. Res.* **2013**, *802*, 159–163. [CrossRef]
25. Kumar, D. Recent advances in tribology of high entropy alloys: A critical review. *Prog. Mater. Sci.* **2023**, *136*, 101106. [CrossRef]
26. Reetz, B. Mikrostruktur und Eigenschaften stranggepresster sowie kaltverformter Messinglegierungen. Ph.D. Thesis, Technische Universität Berlin, Berlin, Germany, 2006.
27. Paulus, A. Tribolayer Formation on Bronze CuSn12Ni2 in the Tribological Contact between Cylinder and Control Plate in an Axial Piston Pump with Swashplate Design. In Proceedings of the International Fluid Power Conference 2016, Dresden, Germany, 8–10 March 2016.
28. Assenova, E.; Kandeva, M. Self-organization and Selective Transfer in Tribology. In Proceedings of the 8th International Conference on Tribology (BALKANTRIB'14), Sinaia, Romania, 30 October–1 November 2014.
29. Reetz, B.; Münch, T. Neue bleifreie Aluminiumbronze für Pleuellager-Anwendungspotential von komplexen Mehrstoffbronzen. *Metall* **2020**, *11*, 431–436.
30. OTTO FUCHS Dülken Material Data Sheets: Alloy OF 2238, available from OTTO FUCHS Dülken on request.
31. *DIN ISO 6892-1:2020-06*; Metallic Materials—Tensile Testing—Part 1: Method of Test at Room Temperature (ISO 6892-1:2019). ISO: Geneva, Switzerland, 2019.
32. Taslicukur, Z.; Altug, G.S.; Polat, S.; Atapek, S.H.; Türedi, E. A Microstructural Study on CuSn10 Bronze Produced by and and Investment Casting Techniques. Conference Paper. 2012. Available online: https://www.researchgate.net/publication/267602750_A_microstructural_study_on_CuSn10_bronze_produced_by_sand_and_investment_casting_techniques (accessed on 15 May 2024).
33. Anantapong, J.; Uthaisangsuk, V.; Suranuntchai, S.; Manonukul, A. Effect of hot working on microstructure evolution of as-cast Nickel Aluminum Bronze alloy. *Mater. Des.* **2014**, *60*, 233–243. [CrossRef]
34. Böhm, J.; Linhardt, P.; Strobl, S.; Haubner, R.; Biezma, M.V. Microstructure of a heat treated Nickel-Aluminum Bronze and its corrosion behavior in simulated fresh and sea water. *Mater. Perform. Charact.* **2016**, *5*, 689–700. Available online: https://www.researchgate.net/publication/308044348_Microstructure_of_a_Heat_Treated_Nickel-Aluminum_Bronze_and_Its_Corrosion_Behavior_in_Simulated_Fresh_and_Sea_Water/link/5f5a1cd7299bf1d43cf94f4f/download?_tp=eyJjb250ZXh0Ijp7ImZpcnN0UGFnZSI6InB1YmxpY2F0aW9uIiwicGFnZSI6InB1YmxpY2F0aW9uIn19 (accessed on 15 May 2024). [CrossRef]
35. Meigh, H. *Cast and Wrought Aluminium Bronzes: Properties, Processes and Structure*; CRC Press: Boca Raton, FL, USA, 2018.
36. Soares, D.; Vilarinho, C.; Silva, R.; Vasques, A.; Castro, F. Influence of the Iron Content on the Solidification Behaviour of Cast Aluminium Bronze Used in Marine Applications. Inter-national Congress on Advanced Materials, Their Processes and Applications, Munique. Available online: https://repositorium.sdum.uminho.pt/bitstream/1822/2190/1/Munique%202001.pdf (accessed on 11 March 2024).
37. Sushanth Poojary, S.; Marakini, V.; Rao, R.N.; Vijayan, V. Enhancing microstructure and mechanical properties of nickel aluminium bronze alloy through tin addition. *Sci. Rep.* **2023**, *13*, 16907. [CrossRef] [PubMed]
38. Bauser, M. *Strangpressen*; Beuth Verlag GmbH: Berlin, Germany, 2011.
39. Hall, E.O. The deformation and ageing of mild steel: III Discussion of results. *Proc. Phys. Soc. B* **1951**, *64*, 747–753. [CrossRef]
40. Gottstein, G. *Physikalische Grundlagen der Materialkunde*; Springer: Berlin/Heidelberg, Germany, 2007.
41. Li, Y.; Bushby, A.J.; Dunstan, D.J. The Hall-Petch Effect as a Manifestation of the General Size Effect. Available online: https://arxiv.org/pdf/1507.01223 (accessed on 15 May 2024).
42. Gummert, H.-J. *Drawing: The Production of Wires, Bars and Tubes*; Text Team Medien und Druck: Detmold, Germany, 2006.

43. Vollert, F.; Lüchinger, M.; Schuster, S.; Simon, N.; Gibmeier, J.; Kern, K.; Schreiner, M.; Tillmann, W. Experimental and numerical analyses of residual stresses induced by tube drawing. *J. Strain Anal. Eng. Des.* **2018**, *53*, 364–375. [CrossRef]
44. Palkowski, H.; Brück, S.; Pirling, T.; Carradò, A. Investigation on the Residual Stress State of Drawn Tubes by Numerical Simulation and Neutron Diffraction Analysis. *Materials* **2013**, *6*, 5118–5130. [CrossRef] [PubMed]